10-2013

The Biological Impact of Concurrent Exposure to Metallic Nanoparticles and a Static Magnetic Field

Kristen K. Comfort
University of Dayton, kcomfort1@udayton.edu

Elizabeth I. Maurer
Air Force Research Laboratory

Saber M. Hussain
Air Force Research Laboratory

The Biological Impact of Concurrent Exposure to Metallic Nanoparticles and a Static Magnetic Field

Kristen K. Comfort[1,2], Elizabeth I. Maurer[1], Saber M. Hussain[1]*

[1]Molecular Bioeffects Branch, Human Effectiveness Directorate, Air Force Research Laboratory, Wright-Patterson AFB, OH 45433, USA

2Department of Chemical and Materials Engineering, University of Dayton, Dayton, OH 45469 USA

Tel.: +1 937-904-9517

Fax: +1 937-904-9610

Saber.hussain@wpafb.af.mil

Running Title: Bioeffects Following SMF and NP Co-exposure

Additional supporting material may be found in the online version of this article

Grant Sponsor: Portions of this work were funded by the 711th HPW/AFRL Chief Scientist Seedling Program, Tier I and the Air Force Surgeon General. K.K.C. was supported through a National Research Council post-doctoral fellowship, funded through the Air Force Office of Scientific Research, and through the Oak Ridge Institute for Science and Education. E.I.M. is funded through the Henry M Jackson Foundation.

Abstract The rapid advancement of technology has led to an exponential increase of both nanomaterial and magnetic field utilization in applications spanning a variety of sectors. While extensive work has focused on the impact of these two variables on biological systems independently, the existence of any synergistic effects following concurrent exposure has yet to be investigated. This study sought to ascertain the induced alterations to the stress and proliferation responses of the human adult low calcium high temperature keratinocyte (HaCaT) cell line by the application of a static magnetic field (approximately 0.5 or 30 mT) in conjunction with either gold or iron oxide nanoparticles for a duration of 24 h. By evaluating targets at a cellular, protein, and genetic level a complete assessment of the HaCaT response was generated. A magnetic field dependent proliferative effect was found (~15%) which correlated with a decrease in reactive oxygen species and a simultaneous increase in ki67 expression; all occurring independently of nanoparticle presence. Furthermore application of a static magnetic field was able to counteract the cellular stress response induced by nanoparticle exposure through a combination of decreased reactive oxygen species production and modification of gene regulation. Therefore we conclude that while these variables each introduce the potential to uniquely influence physiological events, no negative synergistic reactions were identified.

Keywords: Static Magnetic Field, Superparamagnetic iron oxide nanoparticle, Gold nanoparticle, Cellular Stress, Gene Regulation

Introduction

The explosive development of nanotechnology has resulted in the incorporation of numerous nanomaterials into everyday products and applications. Their unique physico-chemical properties make nanomaterials attractive for applications in a diverse number of specialties, including electronics, energy, personal care, and medicine. For example, gold, silver, and copper nanoparticles (NPs) are all employed as high conductivity elements in circuits and electronic devices [Wang et al., 2004; Li et al., 2005]. Furthermore, numerous NPs, including aluminum, boron, iron, and titanium, are highly combustive and are being integrated into fuels and propellants to increase their efficiency [Yetter et al., 2009]. Silver NPs are being robustly utilized as an antimicrobial agent in both the consumer and medical sectors, with specific applications including medical bandages and devices, clothing, food packaging, and cosmetics [Zhang et al., 2008; Wijnhoven et al., 2009]. It logically follows that as the prevalence of nanomaterials in consumer goods increases, the risk of nanomaterial exposure escalates proportionately. To ascertain the potential hazards of nanomaterial introduction on a physiological system, numerous studies have assessed the impact of various types, sizes, and shapes of nanomaterials on biological effects (bioeffects) [Hussain et al., 2005; Braydich-Stolle et al., 2009; Braydich-Stolle et al., 2010; Schaeublin et al., 2011]. The results of these investigations have found that nanomaterials are able to severely influence an *in vitro* environment with noted outcomes involving cytotoxicity, augmentation of cellular stress, and activation of the inflammatory and immune responses. However, as these cellular implications are dependent on numerous factors including nanomaterial composition, shape, size, and surface coating, the true impact of nanomaterials has yet to be satisfactorily elucidated.

In a similar fashion, the rate of human exposure to magnetic fields (MFs) has substantially increased in recent years, with production arising from a wide variety of sources, including personal electronics, appliances, and power lines. This rapid technological advancement has sparked public inquiry into the potential health risks associated with extensive MF exposure [Kheifets, 2001; Karasek and Lerchl, 2002]. Considerable investigation has sought to answer that question by evaluating the ability of a MF, of various strengths and types, to influence cellular events and targeted bioeffects [Dini and Abbro, 2005; Miyakoshi, 2005]. While the potential for serious ramifications from MF exposure has been identified, the mechanism and degree of interference is not yet completely understood. However, to date, no study has systematically investigated the consequences of concurrent

exposure to nanomaterials and a static MF at low, incidental levels on a biological environment.

As both MFs and NPs possess unique properties that can target and alter cellular functions, it is highly probable that their simultaneous application could produce a combinatorial bioeffect; a cellular outcome that does not occur under the influence of either NPs or a MF alone. Numerous studies have reported that NPs induce a cytotoxic response through the induction of oxidative stress and DNA damage [Carlson et al., 2008; Lewinski et al., 2008]. Even in the absence of cellular death, NPs have been shown to augment intracellular stress levels and modify genetic regulation [Singh et al., 2009; Comfort et al., 2011]. Analogous to NPs, MFs have been proven to modulate *in vitro* viability, redox systems, and gene regulation [Dini and Abbro, 2005; Frahm et al., 2010]. Consequently, as people continuously encounter scenarios that involve MF and NP co-exposure, the need for the determination of synergistic bioeffects is of the utmost importance to ascertain the potential impact on human health.

The goal of this study was not to investigate the effects of one stimulus or the other, as that has previously been explored, but to establish if any cooperative bioeffects arose in the human adult low calcium high temperature keratinocyte (HaCaT) cell line following cellular introduction of both NPs and a static MF. The HaCaT line was selected due to the considerations that contact is a primary mechanism of nanomaterial exposure and a MF would have the greatest impact on the skin surface; owing to the fact that the flux of a MF dramatically reduces as a function of distance from its source. To identify the role of field strength, cells were exposed to either a 0.53 mT or 31.3 mT static MF (hereafter referred to as 0.5 and 30 mT for brevity); both of which are flux intensities one would encounter on a daily basis. Due to their general biocompatibility, use in numerous applications, and magnetic properties, super paramagnetic iron oxide nanoparticles (SPIONs) and gold nanoparticles (Au-NPs) were the nanomaterials of choice for this investigation [Lewinski et al., 2008]. Furthermore, a comprehensive survey of bioeffects was evaluated, at a cellular, protein, and genetic level, to generate a complete picture of the HaCaT stress and proliferative responses. Our results establish that exposure to Au-NPs or SPIONs in conjunction with a static MF, both at incidental levels, did not result in an overtly negative synergistic cellular response.

Materials and Methods

NP Synthesis and Characterization

The SPIONs were purchased from Nanocs (New York, NY, USA) in concentrated, solution form. The citrate stabilized gold nanospheres were synthesized in-house using a previously described wet chemistry method [Grabar et al., 1995] and functionalized with polyethylene glycol [Liu et al., 2007]. Concentrations of the NP stocks were determined through inductively coupled plasma mass spectrometry on a Perkin Elmer NexION 300D (Waltham, MA, USA). Primary NP size and spherical morphology were verified using transmission electron microscopy (TEM) on a Hitachi H-7600 microscope (Tokyo, Japan). Dynamic light scattering (DLS) and zeta potential analyses were used to assess NP agglomeration and surface charge, respectively, on a Malvern Zetasizer Nano ZS (Worcestershire, UK) [Murdock et al., 2008]. NP solutions used for dosing were made up fresh prior to each experiment to avoid extensive agglomeration.

Cell Culture and MF Exposure

The human keratinocyte HaCaT cell line was a kind gift from the Army Research Laboratory (Adelphi, MD, USA), and was maintained in Roswell Park Memorial Institute (RPMI) 1640 medium supplemented with 10% fetal bovine serum and 1% penicillin/streptomycin (American Type Cell Culture, Manassas, VA, USA). HaCaTs are a spontaneously derived immortalized cell line, and therefore display no tumorigenesis characteristics. During experimentation, cells were seeded in either 6- or 96-well tissue culture plates or a 2-well chambered slide (Fisher Scientific, Pittsburgh, PA, USA) and returned to the incubator for the indicated duration and exposure conditions.

The static MFs were generated by high-temperature ferrite permanent bar magnets (McMaster-Carr, Cleveland, OH, USA). The HaCaT cells were exposed to these MFs by the placement of culture dishes on top of the magnets within an incubator maintained at 37°C and 5% CO_2. A schematic of the SMF cellular exposure scenario is shown in Figure 1. The magnetic poles were located on the longitudinal ends of the magnets, thus generating a traditional inhomogeneous magnetic field running from north to south. The rectangular magnets utilized had physical dimensions of 127 x 76 x 1.3 mm and 152 x 10.2 x 13 mm for the low and high MF conditions, respectively. Based on the number of experimental wells the cellular surface area was calculated to be 1540 mm^2 (36 mm length x 42.7 width), which correlates to 16% and 9.9% of the surface area of these permanent magnets. A centralized location for placement of experimental wells was denoted on the magnets, and within that

area the maximum field strength was measured on a LakeShore 410 Gaussmeter with a transverse Hall probe (Westerville, OH, USA). To accurately reflect the MF exposure encountered by the HaCaTs, the determination of the maximum flux density was carried out at a distance of 4 mm above the magnet surface, which is equal to that of the cell culture height. The average maximum flux values were based on the measurement of 20 spatial locations within the designated cellular placement area and found to be 0.53 ± 0.03 and 31.3 ± 0.23 mT, for the low and high MF conditions, respectively. Therefore, even though the generated field was inhomogeneous, the cellular exposure area was small enough that the MF strength encountered by the HaCaT cells was relatively constant; within approximately 5% for the 0.5 mT and 1% for the 30 mT conditions. While the actual MF field strengths are slightly higher, for the sake of brevity and simplicity, the 0.53 mT and 31.3 mT fields will be referred to as 0.5 mT and 30 mT for the remainder of this study.

In the control conditions, cells were prepared in the same manner but were not exposed to the static MF. Control dishes were placed in a separate, but identical, incubator to remove them from the influence of additional magnetic flux. The cells exposed to the 0.5 and 30 mT MF were placed in the upper left and lower right corner of the incubator, respectively. At this distance it was verified, using the same probe as previously mentioned, that the magnetic fluxes did not interfere with one another.

NP Uptake and Cellular Interactions

For cellular association, 2 x 10^5 cells were plated per chamber on a 2-well chambered slide and grown for 24 h, after which they were exposed to 15 μg/mL of NPs and the stated MF condition for an additional 24 h. The cells were then fixed with 4% paraformaldehyde and incubated with Alexa Fluor 555-phalloidin (Invitrogen, Carlsbad,CA, USA) for actin staining and 4',6-Diamidino-2- phenylindole (DAPI) for nuclear staining (Invitrogen). The slides were then sealed and imaged using a CytoViva 150 ultraresolution attachment on an Olympus BX41 microscope (Aetos Technologies, Auburn, AL, USA).

For uptake studies 8 x 10^5 cells were plated per well in a 6-well plate, equilibrated for 24 h, then dosed with 15 μg/mL of NPs and either a 0 or a 30 mT static MF for a duration of 24 h. Thereafter, the cells were fixed in 2% paraformaldehyde/2% glutaraldehyde (Electron Microscope Sciences (EMS), Hartfield, PA, USA) for 2 h, stained with a 1% osmium tetroxide (EMS), and dehydrated using increasing ethanol concentrations. Cell pellets were then cured for 16 h at 60 °C in LR White Resin (EMS). Finally, the cell samples were thin-sectioned on an EM UC7 Leica ultramicrotome (Wetzlar, Germany) and visualized *via* TEM.

Cell Proliferation

Cell proliferation was assessed using the CellTiter 96 Aqueous One Solution (Promega, Madison, WI, USA) which monitors mitochondrial function. Cells were seeded into a 96-well plate at a concentration of 5000 per well and the following day treated with the stated NP and MF conditions. After 24 h the cells were washed and viability was determined in accordance with the manufacturer's protocol, including an initial absorbance reading to account for NP presence. Control samples were cells without either NP or MF treatment.

Reactive Oxygen Species Production

The generated reactive oxygen species (ROS) was monitored via the fluorescent probe dichlorofluorescein diacetate (DCFH-DA, Invitrogen). Cells were seeded at 7500 cells per well in a 96-well plate and adhered overnight. On the day of experimentation, the cells were washed and treated with 100 µM DCFH-DA for 30 m, washed again, and dosed with the specified combination of NPs and MFs. After 24 h incubation the fluorescence was measured on a SpectraMAX Gemini Plus microplate reader (Molecular Devices, Sunnyvale, CA, USA). Wells without NPs or MF exposure served as the negative control. To verify the DCFH-DA probe was properly functioning, cells treated with hydrogen peroxide were used as a positive control.

Ki67 Evaluation

The expression of ki67 was monitored with through the ki67 Cell Proliferation Kit by Thermo Scientific (Waltham, MA, USA). Cells were seeded onto a 96-well plate at a density of 7500 cells per well in growth media, adhered overnight, and then exposed to the stated combination of NPs and MF. After 24 h, the cells were washed, fixed with 4% formaldehyde, permealized, and stained with antibodies specific to ki67, all in accordance with the manufacturer's protocol. The fluorescence intensity was measured on a SpectraMAX Gemini Plus microplate reader.

Gene Expression Analysis

For real time polymerase chain reaction (RT-PCR) analyses, cells were plated at a density of 8×10^5 cells per well in a 6-well plate and cultured in growth media overnight. The cells were then washed and dosed with 5 µg/mL of Au-NPs or SPIONs and exposed to the specified MF for 24 h. The RNA was then isolated from each culture using the RNAeasy Mini Kit from Qiagen (Valencia, CA, USA) and quantified with the NanoDrop ND-1000 spectrophotometer (Thermo Scientific). The RNA samples were processed and converted to cDNA using the RT2 First Strand kit from SA Biosciences (Frederick, MD, USA), and the

human Stress and Toxicity PCR Array (SA Biosciences) was run in accordance with the manufacturer's protocol.

Statistical Analysis

Data is expressed as the mean ± the standard error of the mean (SEM). A one-way ANOVA analysis was run using Graph Pad Prism (La Jolla, CA, USA) followed by a Bonferroni adjustment to determine statistical significance with an asterisk denoting a p-value ≤ 0.05. The data collected from the PCR arrays was analyzed with the aid of the SABioscience software. The data reported for gene expression analysis passed two quality assurance criteria, with respect to data analysis. Firstly, the fold regulation of an experimental condition was statistically significant, a p-value ≤ 0.05, when directly compared against the control, which was no NP and no SMF stimulation (n=3 for both experimental sets). Secondly, of these statistically significant sets, only the genes that displayed a fold regulation greater than 2.0 were included.

Results

Nanoparticle Selection and Characterization

When designing this study the main consideration for NP selection was the potential for influence by a MF. Owing to their superparamagnetic properties, SPIONs will indisputably be manipulated by the presence of a static MF. As many metallic NPs demonstrate magnetic properties considerably different from their bulk counterparts, the sensitivity of nano-gold was of great interest, as gold has been shown to magnetize when situated directly with a MF. An additional factor involved in NP selection was their general prevalence in consumer, medical, and industrial applications; as commonly utilized particles incur the highest exposure levels. Both SPIONs and Au-NPs are frequently employed in the medical field and incorporated into consumer products, with applications including enhanced imaging techniques, sensor development, and drug delivery systems [Gupta and Gupta, 2005; Ghosh et al., 2008]. Lastly, as the impact of SPIONs and Au-NPs on a cellular system has been extensively investigated; [Mahmoudi et al., 2009; Khlebtsov and Dykman, 2011], it created a baseline of expected HaCaT responses to these NPs.

As previous investigations have demonstrated that a slight alteration in nanomaterial properties can dramatically impact the dependent bioeffects, it is essential that a proper and extensive characterization of nanomaterials be performed prior to introduction into a physiological system [Hussain et al., 2009; Rivera Gil et al., 2010]. Therefore, the SPIONs

and Au-NPs underwent the standard battery of characterization tests including; verification of primary size and spherical morphology, determination of agglomeration patterns, and an assessment of surface charge (Table 1). Both the Au-NPs and SPIONs demonstrated a uniform, spherical morphology (Fig. 2) and a primary size of approximately 10 nm as determined from TEM imaging. Previous studies have determined that all nanomaterials will agglomerate to some extent when dispersed in various fluids, due to their unique surface chemistries; therefore dynamic light scattering (DLS) was performed to assess an effective agglomerate size in both water and media. As anticipated, some NP agglomeration did occur, however not to an extreme degree, approximately 3-5 times of the primary size, and similar patterns were observed for both Au-NPs and SPIONs. The uniformity of agglomerate size and particle quality can be further assessed through the polydispersity index (PdI) value that is generated during DLS analysis. The PdI, which is valued from 0 to 1, is a measure of the "broadness" of agglomerate size distribution, a general indication of NP quality. To have a good measure of confidence in a NP sample, a PdI of less than 0.5 is traditionally required. As seen in Table 1, the PdI values for both Au-NPs and SPIONs are significantly less than 0.5, indicating that the agglomerates are uniform in addition to being of minimal size. Lastly, the zeta potential indicated that both the NPs exhibited a negative surface charge following dispersion in water as well as in media. The alteration of zeta potential in media is known to be caused the formation of a protein corona around the particles in the presence of serum, which then dictates the external charge of the agglomerates [Lynch et al., 2009]. As surface charge of the particles is critical to how they interact with the cells it is important to note of any substantial differences, of which none were identified.

Evaluation of NP-HaCaT Interactions Under MF Influence

As the mechanism of cellular interaction frequently dictates the resultant bioeffects, the initial objective was to establish whether a static MF impacted how Au-NPs or SPIONs associated with HaCaT cells. Firstly, qualitative NP-cellular coupling was assessed *via* ultrahigh resolution microscopy coupled with fluorescence staining. MFs have been shown to influence cell morphologies [Chionna et al., 2005], but HaCaT control cells appear unaltered following stimulation with a MF (Fig. 3a). As depicted in Figure 3b, Au-NPs readily associated with HaCaT cells whether under the influence of a MF or not. Furthermore, particle clustering was identified in both circumstances suggesting that Au-NP-HaCaT behavior was independent of MF presence. Additionally, as anticipated, SPIONs cluster together following MF exposure as indicated with grey arrows (Fig. 3c). On their own, SPIONs have strong membrane coupling without demonstrating extensive particle

agglomeration, this is in agreement with previous studies [Comfort et al., 2011]. This membrane coupling results in what appears to be a "haze" of nanoparticles over the surface of the cell culture. However, once under the influence of a magnetic flux, bright clusters appear that are indicative of particle grouping.

As MF-dependent NP clustering could alter the way that cells perceive them, the investigation into cellular–nano interactions was taken one step further and NP uptake patterns were evaluated. Representative TEM images of control HaCaT cells demonstrated no obvious alterations following MF introduction (Fig 4a). As shown in Figure 3b, Au-NPs were readily internalized by HaCaT cells without the presence of a static MF, through what appears to be an endocytosis mechanism, though the exact form of endocytosis is unknown. Following exposure to the 30 mT MF, Au-NPs were still clearly taken up by the cells, indicating that MF application did not block particle internalization. The lack of SPION internalization without a MF (Fig. 4c) is in agreement with the previous microscopy results, in which SPIONs appeared distributed on the cell surface (Fig. 3c) as well as previously published experimentation [Comfort et al., 2011]. However, even following MF dependent SPION clustering, no perceivable uptake occurred. Therefore, while these results demonstrated significant SPION grouping, no considerable variations of cellular–nano interactions transpired during exposure to a 30 mT static MF.

Bioeffects at the Cellular Level: Viability and Reactive Oxygen Species Assessments

As previously mentioned, Au-NPs and SPIONs are renowned for their general biocompatibility, with minimal cytotoxic effects. The impact of a MF on an *in vitro* system is more debatable with both proliferative and apoptotic effects reported, depending on the cell line [Tenuzzo et al., 2006]. Following 24 h of concurrent stimulation by a MF and 5 µg/mL of either Au-NPs or SPIONs, HaCaT cells exhibited a proliferative effect (~10-15%) that was dependent solely on the presence of a static MF (Fig. 5). Interestingly, this proliferation was independent of the field strength with the same cell growth observed in the presence of both 0.5 and 30 mT magnets, a 60-fold difference. Most notably, identical proliferative patterns were observed in the presence of no NPs, Au-NPs and SPIONs, indicating no negative synergy relative to HaCaT viability. Through previously completed investigations, it has been identified that a large percentage of the observed nano-based cellular responses are directly tied to the concentration of particles used. Therefore, to identify if NP dosage had a role in joint NP-MF bioeffects, this trial was repeated with a higher NP concentration (Fig. S-1). However, even at significantly increased NP concentrations comparable results were

observed, re-emphasizing the conclusion that the identified proliferative effect is a sole product of MF application to HaCaT cells.

One factor that has been shown to strongly correlate with a culture's growth rate is the amount of stress that the cells are incurring; which was assessed through the production of reactive oxygen species (ROS), a recognized marker of cellular distress [Fiers et al., 1999]. SPIONs and MFs on their own have been shown to impact the intracellular redox balance [De Nicola et al., 2006; Singh et al., 2012], and this was reproduced in the HaCaT cell line with a marked increase and decrease, respectively, in ROS levels (Fig. 6). Furthermore, results demonstrated that a static MF was able to counteract the ROS production by SPIONs, returning quantities to an approximate basal level. To a similar extent, approximately 15-20%, MFs attenuated ROS levels in conjunction with control cells and Au-NPs. Analogous to the viability results, this bioeffect was independent of MF strength and similar patterns in ROS levels were seen following exposure to a higher nanoparticle dose (Fig. S-2). Together, these results demonstrate that even in conjunction with NPs, a static MF is capable of inducing a proliferative HaCaT response through the decrease of intracellular ROS production.

Bioeffects at the Protein Level: Augmented ki67 Production

On the protein level, the quantity of ki67, a recognized protein marker for cell proliferation [Gerdes et al., 1983], was assessed following concurrent NP and MF exposure to validate the previous proliferative results. For all NP variations, a substantial increase in ki67 expression, 15-20%, was detected following the introduction of a MF (Fig. 7), directly correlating with the observed HaCaT MF-dependent growth. As seen with earlier experimentation, this ki67 increase appeared to be independent of MF strength and NP presence, and solely reliant on the presence of a MF.

Bioeffects at the Genetic Level: Alterations in Gene Regulation

Lastly, alterations to HaCaT gene regulation were investigated following simultaneous NP and MF exposure. To determine if a correlation existed between genetic modifications and the observed stress and proliferative responses, a gene array was selected that specifically focused on stress and toxicity related genes. This RT-PCR array, which examines 84 genes known to be involved in the cellular stress and toxicity responses, was executed following NP exposure and repeated for a culture under the influence of NPs and a 30 mT MF. The data sets were then compared directly against one another to elucidate the influence of a MF on gene transcription; these findings are summarized in Table 2. The samples that underwent NP exposure demonstrated a MF dependent upregulation in proliferative genes with a

simultaneous downregulation in apoptotic genes. Furthermore, the observed alterations are predominantly comparable for Au-NP and SPION, however SPION samples were more prone to downregulate apoptotic genes. This finding was not surprising, however, as Au-NPs generally do not induce an apoptotic response. Control samples were run without NP exposure, and while similar trends of were seen following the application of a MF, none of the genes in the array met the criteria of a minimum fold regulation of 2.0 or greater; demonstrating that these results are a combinatorial bioeffect and not resultant solely on the presence of a MF.

Discussion and Conclusion

NP-MF Impact on HaCaT Viability and Stress

The goal of this study was to identify potential hazards following low level exposure to both NPs and a static MF. Although not overtly negative, this study identified a variation of bioeffects in the HaCaT cell line as a result of SPION or Au-NP dosing in conjunction with the application of a MF. No significant changes in the cellular morphology or uptake patterns (Fig. 3 and Fig. 4) indicated that the observed alterations can be directly attributed to the MF-NP interactions and not the cellular-nano association. Firstly a significant increase in proliferation was observed following the application of a MF (Fig. 5). Subsequent experimentation indicated that this proliferation was stimulated by a considerable reduction in ROS levels (Fig. 6), increased ki67 expression (Fig. 7), and alteration to gene regulation (Table 2). It was recently reported that a static MF upregulated gene expression directly responsible for DNA repair and cell proliferation in human umbilical vein endothelial cells (HUVEC) [Polidori et al., 2012] thereby indicating that this phenomenon is not unique to HaCaTs. Our study further revealed that MF exposure increased the expression of C-X-C motif chemokine 10 (CXCL10), interleukin-6 (IL-6), lymphotoxin alpha (LTA), and tumor necrosis factor (TNF) in NP treated HaCaT cells, all of which are key players in the inflammatory response. However, CXCL10, IL-6 and LTA have also been linked to enhancing cellular proliferation [Krueger et al., 1991; Calmon-Hamaty et al., 2011] and, we presume, aid in the enhancement of the observed MF-dependent proliferative effect. This is noteworthy as NPs have previously been shown to increase the inflammatory response [Braydich-Stolle et al., 2010; Nishanth et al., 2011] and these results suggest a further augmentation of pro-inflammatory cytokine secretion by the application of a MF. Taken

together, these facts suggest that the immune and inflammatory systems may be sensitive to concurrent MF and NP exposure and require further exploration.

The results presented in this study pose very intriguing questions as to a potential role for MFs used in combination with NPs and the resultant effect on the cellular stress response. It is established that many NPs, including SPIONs, increase intracellular stress following their introduction. Most interestingly, we revealed the ability of a static MF to counteract this SPION-induced, augmented stress and return ROS levels to a near basal quantity. We hypothesize that the MF presence is somehow supplementing the cell's natural antioxidant abilities, as this MF ability has previously been shown [Wang et al., 2008]. However, SPIONs alone demonstrated no alteration to HaCaT viability, indicating that the cells were able to manage the increased stress load on their own. As such, it would be worthwhile to evaluate the degree of MF induced stress reduction and potential recovery of cell viability in conjunction with a NP that is a recognized inducer of ROS dependent cytotoxicity, such as nano-silver [Carlson et al., 2008].

Variable Response to NPs and MFs

A recent study completed by Bae et al. [2011] discovered a cytotoxic, synergistic effect when ferucarbotran nanoparticles were used with a 0.4 T MF on hepatocyte cells; specifically replicating an MRI scenario. The authors found that the strong MF increased NP agglomeration and cellular uptake, resulting in dramatically higher ROS levels and leading to cell death. However, a hallmark of MF-induced bioeffects has been that results are dependent on factors such as cell line, MF strength, and class of MF [Dini et al., 2005; Tenuzzo et al., 2006]. This variability has evidently been retained when assessing combinatorial bioeffects with nanomaterials. While the authors of Bae et al. encountered a negative response, our study indicates no considerable NP-MF toxicity, but rather the potential for a cooperative effect between MFs and NPs; as demonstrated by the ability of the MF to counteract SPION dependent ROS production. While several distinct differences exist between these two novel studies, including field strength (0.4 T *vs.* 0.5 and 30 mT), cell model (murine hepatocytes *vs.* human keratinocytes), and NP biocompatibility (toxic *vs*. non-toxic) both reports examined the effects of simultaneous MF and NP exposure on a biological system. Therefore, we believe that these two investigations together illuminate the potential, both positive and negative, of combining the stimulus effects of NPs and static MFs for biological purposes. Furthermore, these results warrant further extensive investigation into this rapidly growing area of public concern and scientific inquiry.

In conclusion, this study evaluated the combinatorial bioeffects at cellular, protein, and genetic levels in HaCaT cells following the introduction of Au-NPs or SPIONs in the presence of a static MF. Under the conditions examined in this study, we identified modifications in the proliferative response, ROS production, and gene regulation, but none indicate an explicitly negative cellular response. On the contrary, this work demonstrated that a static MF is capable of counteracting the augmented stress levels often associated with nanomaterial introduction. While we identified no overtly damaging synergistic cellular responses during a co-exposure scenario of incidental levels of NPs and a MF, this report has barely scratched the surface on the investigation into combinatorial effects on a physiological system, and we believe merits further exploration in this area to fully elucidate any potential interactions that may arise.

Acknowledgments The authors would like to thank Ms. Emily Breitner for assistance with the CytoViva imaging and Mr. Bradley Stacy for providing the gold nanoparticles.

References

Bae JE, Huh MI, Ryu BK, Do YK, Jin SU, Moon MJ, Jung JC, Chang Y, Kim E, Chi SG, Lee GH, Chae KS. 2012. The effect of static magnetic fields on the aggregation and cytotoxicity of magnetic nanoparticles. Biomaterials 32:9401-9414.

Braydich-Stolle LK, Schaeublin NM, Murdock RC, Jiang J, Biswas P. 2009. Crystal structure mediates mode of cell death in TiO(2) nanotoxicity. J Nanopart Res 11:1361-1374.

Braydich-Stolle LK, Speshock JL, Castle A, Smith M, Murdock RC, Hussain SM. 2010. Nanosized aluminum altered immune function. ACS Nano 4:3661-3670.

Calmon-Hamaty F, Combe B, Hahne M, Morel J. 2011. Lymphotoxin alpha stimulates proliferation and pro-inflammatory cytokine secretion of rheumatoid arthritis synovial fibroblasts. Cytokine 53:207-214.

Carlson C, Hussain SM, Schrand AM, Braydich-Stolle LK, Hess KL, Jones RL, Schlager JJ. 2008. Unique cellular interaction of silver nanoparticles: Size-dependent generation of reactive oxygen species. J Phys Chem B 112:13608-13619.

Chionna A, Tenuzzo B, Panzarini E, Dwikat MB, Abbro L, Dini L. 2005. Time dependent modifications of Hep G2 cells during exposure to static magnetic fields. Bioelectromagnetics 26:275-286.

Comfort KK, Maurer EI, Braydich-Stolle LK, Hussain SM. 2011. Interference of silver, gold, and iron oxide nanoparticles on epidermal growth factor signal transduction in epithelial cells. ACS Nano 5:10000-10008.

De Nicola M, Cordisco S, Cerella C, Albertini MC, D'Alessio M, Accorsi M, Bergamaschi A, Magrini A, Ghibelli L. 2006. Magnetic fields protect from apoptosis via redox alteration. Ann NY Acad Sci 1090:59-68.

Dini L, Abbro L. 2005. Bioeffects of moderate-intensity static magnetic fields on cell cultures. Micron 36:195-217.

Fiers W, Beyaert R, Declercq W, Vandenabeele P. 1999. More than one way to die: apoptosis, necrosis and reactive oxygen damage. Oncogene 18:7719-7730.

Frahm J, Mattsson MO, Simko M. 2010. Exposure to ELF magnetic fields modulate redox related protein expression in mouse macrophages. Toxicol Lett 192:330-336.

Gerdes J, Schwab U, Lemke H, Stein H. 1983. Production of a mouse monoclonal-antibody reactive with a human nuclear antigen associated with cell-proliferation. Int J Cancer 31:13-20.

Ghosh P, Han G, De M, Kim CK, Rotello VM. 2008. Gold nanoparticles in delivery applications. Adv Drug Delivery Rev 60:1307-1315.

Grabar KC, Freeman RG, Hommer MB, Natan MJ. 1995. Preparation and characterization of Au colloid monolayers. Anal Chem 67:735-743.

Gupta AK, Gupta M. 2005. Synthesis and surface engineering of iron oxide nanoparticles for biomedical applications. Biomaterials 26:3995-4021.

Hussain SM, Braydich-Stolle LK, Schrand AM, Murdock RC, Yu KO, Mattie DR, Schlager JJ. 2009. Toxicity evaluation for safe use of nanomaterials: Recent achievements and technical challenges. Adv Mater 21:1549-1559.

Hussain SM, Hess KL, Gearhart JM, Geiss KT, Schlager JJ. 2005. In vitro toxicity of nanoparticles in BRL 3A rat liver cells. Toxicol in Vitro 19:975-983.

Karasek M, Lerchl A. 2002. Melatonin and magnetic fields. Neuroendocrinol Lett 23:84-87.

Kheifets LI. 2001. Electric and magnetic field exposure and brain cancer: A review. Bioelectromagnetics 22(Suppl 5): S120-131.

Khlebtsov N, Dykman L. 2011. Biodistribution and toxicity of engineered gold nanoparticles: A review of in vitro and in vivo studies. Chem Soc Rev 40:1647-1671.

Krueger J, Ray A, Tamm I, Sehgal PB. 1991. Expression and function of interleukin-6 in epithelial cells. J Cell Biochem 45:327-334.

Lewinski N, Colvin V, Drezek R. 2008. Cytotoxicity of nanoparticles. Small 4:26-49.

Li Y, Wu Y, Ong BS. 2005. Facile synthesis of silver nanoparticles useful for fabrication of high-conductivity elements for printed electronics. J Am Chem Soc 127:3266-3267.

Liu Y, Shipton MK, Ryan J, Kaufman ED, Franzen S, Feldheim DL. 2007. Synthesis, stability, and cellular internalization of gold nanoparticles containing mixed peptide-poly(ethylene glycol) monolayers. Anal Chem 79:2221-2229.

Lynch I, Salvati A, Dawson KA. 2009. Protein-nanoparticle interactions: what does the cell see? Nat Nanotechnol 4:546-547.

Mahmoudi M, Simchi A, Milani AS, Stroeve P. 2009. Cell toxicity of superparamagnetic iron oxide nanoparticles. J Colloid and Interface Sci 336:510-518.

Miyakoshi J. 2005. Effects of static magnetic fields at the cellular level. Prog Biophys Mol Biol 87:213-223.

Murdock RC, Braydich-Stolle L, Schrand AM, Schlager JJ, Hussain SM. 2008. Characterization of nanomaterial dispersion in solution prior to in vitro exposure using dynamic light scattering technique. Toxicol Sci 101:239-253.

Nishanth PP, Jyotsna RG, Schlager JJ, Hussain SM, Redanna P. 2011. Inflammatory response of RAW 264.7 macrophages upon exposure to nanoparticles: Role of ROS-NF kappa B signaling pathway. Nanotoxicology 5: 502-516.

Polidori E, Zeppa S, Potenza L, Martinelli C, Colombo E, Casadei L, Agostini D, Sestili P, Stocchi V. 2012. Gene expression profile in cultured human umbilical vein endothelial cells exposed to a 300 mT static magnetic field. Bioelectromagnetics 33:65-74.

Rivera Gil P, Oberdorster G, Elder A, Puntes V, Parak WJ. 2010. Correlating physico-chemical with toxicological properties of nanoparticles: The present and future. ACS Nano 4:5527-5231.

Schaeublin NM, Braydich-Stolle LK, Schrand AM, Miller JM, Hutchison J, Schlager JJ, Hussain SM. 2011. Surface charge of gold nanoparticles mediates mechanism of toxicity. Nanoscale 3:410-420.

Singh N, Manshian B, Jenkins GJS, Griffiths SM, Williams PM, Maffeis TG, Wright CJ, Doak SH. 2009. NanoGenotoxicology: The DNA damaging potential of engineered nanomaterials. Biomaterials 30:3891-3914.

Singh N, Jenkins GJS, Nelson BC, Marquis BJ, Maffeis TGG, Brown AP, Williams PM, Wright CJ, Doak SH. 2012. The role of iron redox state in the genotoxicity of ultrafine superparamagnetic iron oxide nanoparticles. Biomaterials 33:163-170.

Tenuzzo B, Chionna A, Panzarini E, Lanubile R, Tarantino P, Di Jeso B, Dwikat M, Dini L. 2006. Biological effects of 6 mT static magnetic fields: A comparative study in different cell types. Bioelectromagnetics 27:560-577.

Wang H, Huang Y, Tan Z, Hu X. 2004. Fabrication and characterization of copper nanoparticle thin-films and the electrocatalytic behavior. Anal Chim Acta 526: 13-17.

Wang HY, Zeng XB, Guo SY, Li ZT. 2008. Effects of magnetic field on the antioxidant defense system of recirculation-cultured Chlorella vulgaris. Bioelectromagnetics 29:39-46.

Wijnhoven SWP, Peijnenburg W, Herberts CA, Hagens WI, Oomen AG, Heugens EHW, Roszek B, Bisschops J, Gosens I, Van De Meent D, Dekkers S, De Jong W, Van Zijverden M, Sips AJ, Geertsma RE. 2009. Nano-silver - a review of available data and knowledge gaps in human and environmental risk assessment. Nanotoxicology 3:109-138.

Yetter RA, Risha GA, Son SF. 2009. Metal particle combustion and nanotechnology. P Combust Inst 32:1819-1838.

Zhang L, Gu FX, Chan JM, Wang AZ, Langer RS, Farokhzad OC. 2008. Nanoparticles in medicine: Therapeutic applications and developments. Clin Pharmacol Ther 83:761-769.

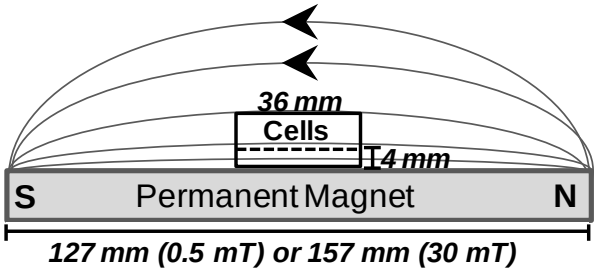

Fig. 1 Schematic of static MF exposure system on HaCaT cells. Cells were positioned at a vertical height of 4 mm above the magnet, indicated by the dashed line. In the longitudinal direction, cell coverage was 36 mm and located in the center of the utilized magnets. Due to their placement and small percentage of occupied magnet surface area, the field strength encountered by the HaCaT cultures is nearly uniform (< 5%).

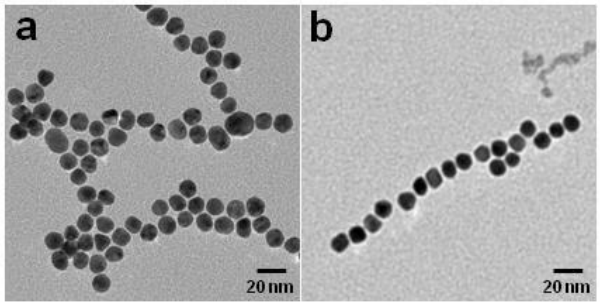

Fig. 2 TEM imaging of original NP stocks of (a) 10 nm gold NPs and (b) 10 nm SPIONs was performed to verify primary nanoparticle size and spherical morphology.

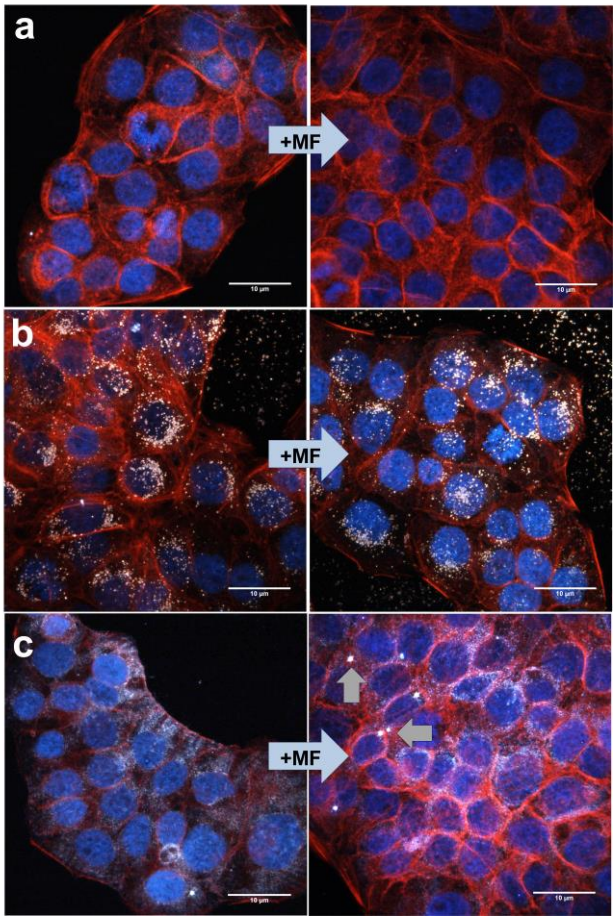

Fig. 3 CytoViva Fluorescent imaging of HaCaT-NP interaction. The influence of a 30 mT static MF on the NP-cellular interface was qualitatively examined with high resolution fluorescent microscopy. Following 24 h of exposure to (a) no NPs, (b) Au-NPs, and (c) SPIONs, the cells were fixed and underwent actin (red) and nuclear (blue) staining with metallic NPs reflecting white. The included arrows indicate the presence of large SPION clusters formed following SMF application.

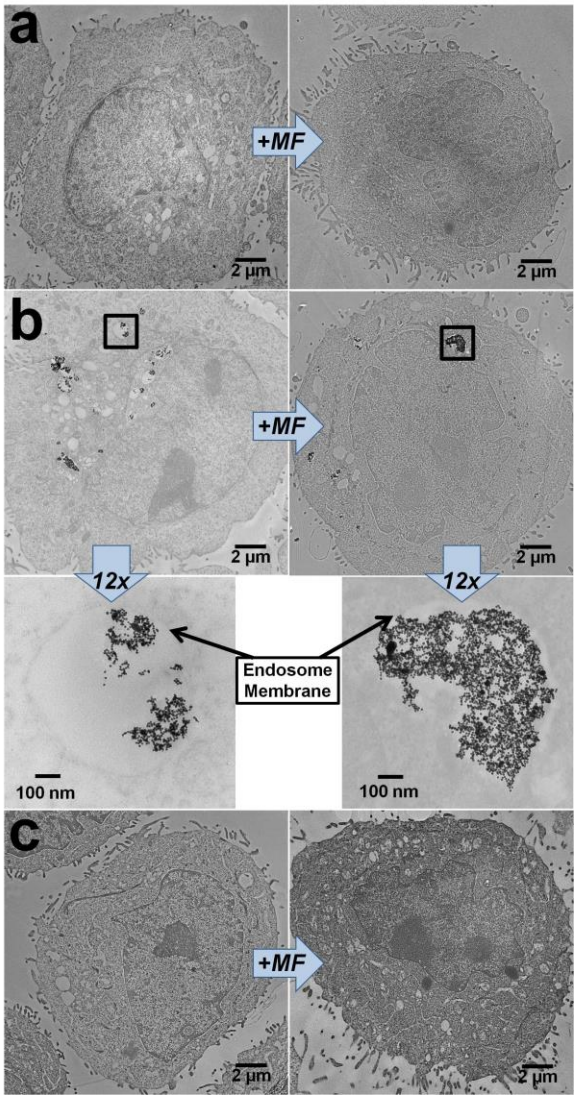

Fig. 4 TEM imaging to evaluate cellular internalization of NPs with and without MF exposure. To visualize if NPs were internalized after 24 h, representative TEM images are shown of HaCaT cells following exposure to (a) no NPs, (b) Au-NPs, and (c) SPIONs before and after application of a 30 mT MF. Images demonstrate significant uptake of Au-NPs, independent of MF status, and no indication of SPION internalization.

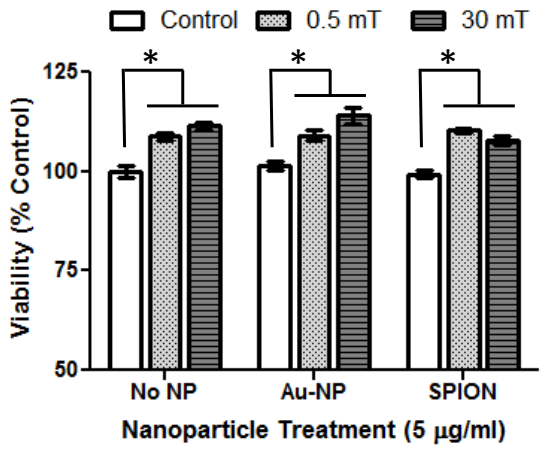

Fig. 5 Impact of simultaneous NP and static MF exposure on HaCaT viability. HaCaT cells were exposed to the stated combination of MF strengths and NPs for 24 h prior to viability evaluation assessed through mitochondrial functionality. Results demonstrated a proliferative response to the MF, independent of field strength and nanoparticle presence. (Represents 3 independent trials, with an asterisk (*) denoting $p \leq 0.05$)

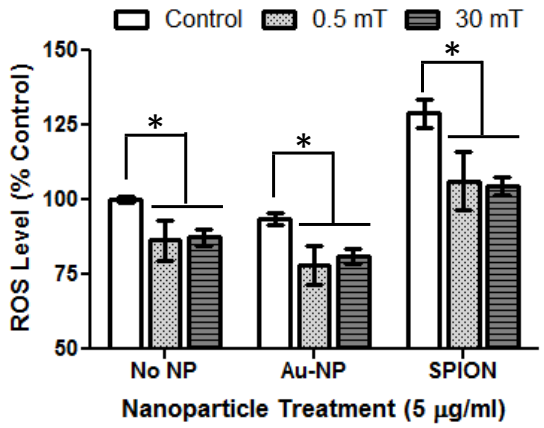

Fig. 6 Reduction in ROS levels by the application of a static MF. ROS production, a marker of cellular stress, was measured 24 h after introduction of the stated combination of NPs and MF strengths. For all NP conditions the presence of a MF significantly reduced ROS levels within the HaCaT cell line. (Represents 3 independent trials, with an asterisk (*) denoting $p \leq 0.05$)

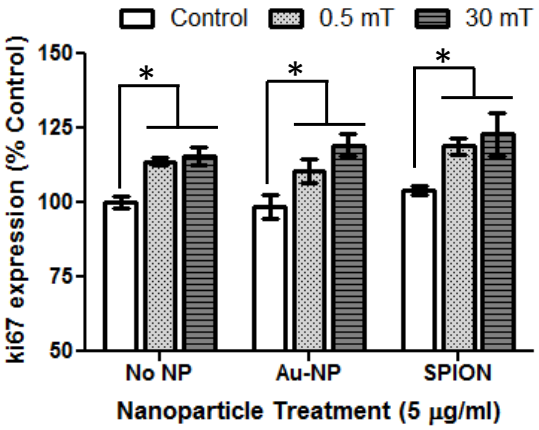

Fig. 7 Enhanced expression of ki67 through static MF exposure. The expression of ki67 protein was evaluated following a 24 h exposure to a combination of a static MF and either gold or SPION nanoparticles. Results demonstrated a significant increase in the intracellular ki67 levels of HaCaT cells after MF application, independent of the presence of NPs. (Represents 3 independent trials, with an asterisk (*) denoting $p \leq 0.05$)

Table 1 Summary of Nanoparticle Characterization

	Primary Size (nm) ± SD	**Agglomerate Size (nm) ± SD**		**Polydispersity Index (PdI)**		**Zeta Potential (mV) ± SD**	
NP		Water	Media	Water	Media	Water	Media
Au-NP	12.19 ± 1.12	37.59 ± 1.82	52.48 ± 1.80	0.241	0.251	-44.33 ± 0.15	-6.22 ± 0.27
SPION	10.17 ± 0.86	30.58 ± 0.10	39.32 ± 0.43	0.141	0.274	-21.07 ± 1.63	-9.91 ± 0.41

Table 2 Alterations to HaCaT gene regulation following concurrent NP and MF exposure

Fold regulation with application of 30 mT MF (vs. 0 mT)				
Gene Symbol	**Functional Group**	**No NP**	**Au-NP**	**SPION**
CASP10	Apoptosis	-	-	-2.02
CXCL10	Inflammatory Response	-	2.77	2.66
DDIT3	Growth Arrest	-	-1.24	-2.01
HSPA6	Protein Repair	-	2.59	3.61
IL6	Inflammatory Response	-	2.16	2.16
LTA	Inflammatory Response	-	2.25	2.70
TNF	Inflammatory Response	-	2.59	1.95
TNFSF10	Apoptosis	-	-	-3.33